


PAPER

[View Article Online](#)
[View Journal](#) | [View Issue](#)Cite this: *J. Mater. Chem. A*, 2024, **12**, 10905

Highly stretchable GR/TPU strain sensor based on one-step electrospun fibrous yarns for wearable devices†

Lei Xing,^a Linze Li,^a Yu Liu,^a Junyi Ren,^b Guilei Guo,^a Yifan Chen,^a Yu Zheng^{*a} and Bin Sun ^{*abc}

Fibrous yarn-based wearable devices have attracted increasing interest in human motion detection. However, challenges remain in the fabrication process and the sensing performance of fibrous yarns. In this work, a highly stretchable graphene (GR)/thermoplastic polyurethane (TPU) strain sensor was prepared based on one-step electrospun TPU nanofibrous yarns. Owing to the electrical conductive pathways constructed by GR, the strain sensor exhibits a large strain range (>140%), a high sensitivity of 46.19, and an excellent durability after more than 10 000 stretching–releasing cycles. With these outstanding properties, textiles based on the strain sensor can be adopted for monitoring various human motions. Moreover, the precise position of an object on the textile can be accurately detected. With a safe temperature of 37.8 °C for the human skin under the maximum operating voltage, the strain sensor shows great potential for the next generation of wearable electronics.

Received 9th January 2024

Accepted 24th March 2024

DOI: 10.1039/d4ta00176a

rsc.li/materials-a

Introduction

Stretchable electronic devices, which are used to monitor various human motions, have been considered a vital component of wearable electronics.^{1–4} In recent years, fibrous yarn- or fabric-based stretchable electronic devices have attracted great interest because of their flexibility, stretchability, breathability, and other advantages. Compared with traditional fibrous film-based devices,^{5–7} yarn- or fabric-based stretchable electronic devices can be more easily integrated into clothing and play an essential role in the field of motion signal and health monitoring.^{8–11} Nowadays, with advantages such as a large specific surface area, high porosity, and long-term durability, fibrous yarn-based devices are used for a wide range of applications, such as strain sensors,¹² pressure sensors,¹³ capacitors,^{14,15} and energy storage devices.¹⁶ However, in most cases, fibrous yarns are fabricated by twisting ready-made individual fibers or complicated equipment is required, increasing the complexity of the fabrication process.¹⁷ Moreover, most conductive yarns cannot be used for textile processing,¹⁸ and sensors made of traditional yarns cannot measure the daily movements of human beings.¹⁹

Recently, flexible/stretchable strain sensors have attracted great interest for human motion monitoring, personalized health monitoring, and human–machine interfaces.^{20–22} In general, such strain sensors are typically fabricated by mixing a polymer matrix/substrate with electrically conductive nanofillers. Polymer materials such as polydimethylsiloxane (PDMS),^{23–25} Ecoflex,^{26,27} and TPU^{28,29} are usually introduced as the substrate, and the nanofillers include carbon materials (*e.g.* carbon nanotubes (CNTs)^{30,31} and GR^{32,33}), metals,^{34,35} conductive polymers,^{36,37} and other materials. Although conductive polymers have perfect mechanical properties, their low electrical conductivity restrict their practical application.³⁸ Metallic conductive fillers have excellent electrical conductive properties, but they usually have the disadvantages of low strain coefficient and easy oxidation. For instance, Yu *et al.*³⁴ prepared liquid metal gallium-based conductive microfiber sensors but low strain coefficients were observed. Zhong *et al.*³⁵ used ultrasound to disperse silver nanowires in polyolefin nanofibrous yarns to prepare strain sensors with a high gauge factor of 13 920 and a minimum detection limit of 0.065%. However, silver nanowires were easily susceptible to oxidation, limiting their long-term applications. Compared with CNTs, graphene has a unique two-dimensional (2D) nature, and its large width-to-thickness ratio renders it a solid platform for electrical and thermal conductance in the whole plane direction.³⁹ Wang *et al.*⁴⁰ prepared a strain sensor by coating graphene oxide (RGO) on a silk fabric and reported excellent performance (good linearity and cycling stability). However, the silk elasticity is relatively low. Despite the high sensitivity, it can only detect up to 10% of the strain, hardly meeting the demand of human skin

^aCollege of Electronics and Information, Qingdao University, Qingdao 266071, PR China. E-mail: zhengyu@qdu.edu.cn; qdusun@qdu.edu.cn^bCollege of Physics, Qingdao University, Qingdao 266071, PR China^{*}Weihai Innovation Research Institute of Qingdao University, Weihai 264200, PR China† Electronic supplementary information (ESI) available. See DOI: <https://doi.org/10.1039/d4ta00176a>

that can produce up to 100% strain during daily exercise.¹⁹ Therefore, there are still challenges in developing simple, low-cost, and scalable manufacturing strategy for strain sensors.

In this work, we report a stretchable strain sensor by integrating GR into TPU fibrous yarns, which were fabricated in a single step using a novel electrospinning equipment. The as-spun TPU fibrous yarns demonstrate high stretchability (>1400%) and large specific surface area. Due to the overlapping of adjacent GR nanosheets, conductive paths are formed, constructing three-dimensional conductive networks within the TPU fibrous yarns. Under stretching, a high sensitivity of 46.19 as well as a superior durability after more than 10 000 stretching–releasing cycles can be achieved. The response mechanism of the strain sensor consists of changes in the distance between adjacent GRs and geometrical changes under the deformation of the TPU mesh and the individual GR-wrapped fibers. It can be applied to detect human motion such as facial expressions, blink, wrist, elbow, and knee bending with fast response, high sensitivity and excellent repeatability. In addition, the precise position of an object can be accurately sensed by preparing it as a sensor array. We hope that our flexible strain sensors will have a promising application in future smart wearable devices.

Experimental

Materials

GR was purchased from Aladdin Biochemical Technology Co. Ltd, Shanghai, China. Polyester-based TPU was provided by Wan Hua Chemical Group Co. Ltd, China. *N,N*-Dimethylformamide (DMF) and tetrahydrofuran (THF) were supplied by Sinopharm Chemical Reagent Co. All materials were used without any further purification.

Preparation of TPU fibrous yarns

TPU powders were dissolved in a mixture of solvents (DMF : THF = 1 : 1), followed by mechanical stirring for 6 hours to obtain a uniform TPU solution with a concentration of 17 wt%. Electrospinning equipment (Model HZ-SX-01) provided by Nuo Kang Environmental Protection Technology Co. Ltd was used to directly fabricate the nanofibrous yarns. The electrospinning parameters used in this work were as follows: the feed rate of the TPU precursor was 3.5 mL h^{−1} on both the left and right sides. A positive voltage was applied to the left side and a negative voltage was applied to the right side (the difference between the positive and negative voltages was 15 kV). The rotational speed of the horn for collecting TPU fibers was 100–210 rpm, and the speed of the TPU yarn collector was 5 rpm. The as-spun yarns were termed as 100@TPU yarn, 120@TPU yarn, 150@TPU yarn, 170@TPU yarn, 190@TPU yarn, and 210@TPU yarn here and after, respectively. The ambient temperature and relative humidity were 27 ± 2 °C and 50 ± 5%, respectively.

Preparation of GR/TPU composite yarns and textiles

A certain quantity of GR was dispersed in deionized water (0.06 wt%) by ultrasonic treatment for 1 hour at 20 °C. After that, single or multiple TPU yarns were immersed into the well-

dispersed GR solution with 2 hours of ultrasonic treatment (sonication frequency of 20 kHz) to obtain GR/TPU yarns. The ultrasonic machine (model FS-450N) was provided by Sheng Xi Ultrasonic Instrument Ultrasonic Instrumentation Co., Shanghai, China. To fabricate the textiles, the GR/TPU yarns were fixed on a knitting machine as warp yarn and commercial polyester yarns were knitted as weft yarn. The GR/TPU strain sensor was obtained after knitting.

Characterization

Mechanical properties were tested on a general-purpose material testing machine (Instron 5300). The surface morphology and cross-section of the samples were observed by scanning electron microscopy (FEI Nova Nano SEM 450). Electrical properties were measured using a Keithley 6485 high resistivity meter system, and the strain–stress curves of the samples were obtained using a dynamic mechanical analyser (Q-800, TA Scientific). The optical photographs of the samples were taken *via* a cell phone (iPhone XS Max). Surface temperature was measured using an infrared thermograph (FOTRIC-226-2, China).

Informed consent was obtained for the experiments involving human participants.

Results and discussion

Basic characteristics

The fabrication process of the GR/TPU strain sensor is shown in Fig. 1a, which mainly consists of electrospinning, ultrasonic treatment and subsequent textile techniques. The electrospinning equipment that can fabricate fibrous yarns in a single step is shown in Fig. 1b. During electrospinning, the solution located at the needle tips was stretched by an electric field force and then formed into a charged jet flow. After the jet flowed away from the spinneret, it was drawn into nanoscale fibers and shifted to the collector at high speed. Then, the horn-shaped collector driven by a motor was designed as a grounding electrode and gathered nanofibers to form a fiber bundle. During the collector rotation, the funnel-shaped collector exerted a twist on the nanofiber bundles to form a stable yarn. Then, the yarns were wound on the yarn rolling device with the traction of the guide roller. Traditionally, fibrous yarns should undergo a series of post-processes from the electrospun fibers, and although there are reports on the direct electrospinning of fibrous yarns,^{41–43} this electrospinning instrument is easier to operate and the electrospun yarn is more uniform. It can be clearly seen that the electrospinning process is highly stable (Movie S1, ESI†), and TPU can be continuously electrospun to form the long fibrous yarn, as shown in Fig. 1c. From the SEM images (Fig. 1d and e), one can see that the as-formed fibrous yarns demonstrate a smooth surface without burr or broken lines and most fibers are aligned along the longitudinal axis of the yarn. Individual TPU fiber without beads is similar to that obtained from traditional electrospinning (Fig. 1f). The as-spun fibrous yarns have excellent flexibility and robustness and can bear a relatively high weight, as shown in Fig. 1g.

The fibrous yarns' morphologies are obviously affected by the horn rotating speed. When the horn was not rotating,

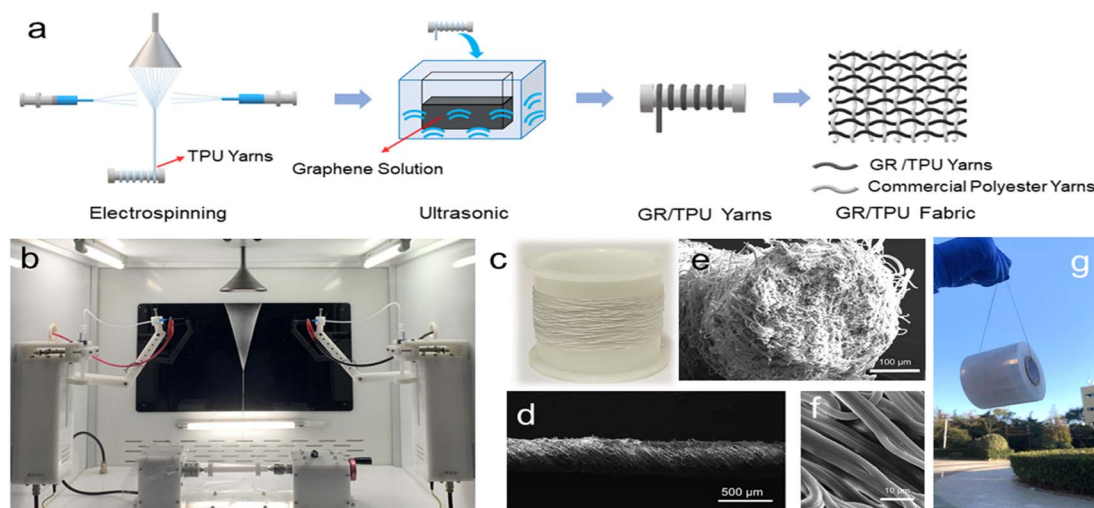


Fig. 1 (a) Schematic of the fabrication process of the GR/TPU strain sensor. (b) Picture of the nano-yarn instrument. (c) Photographs of TPU yarns. (d–f) SEM images of TPU yarns at different magnifications. (e) Cross-sectional SEM image of the TPU yarns. (g) Photograph of GR/TPU yarns hanging an adhesive tape.

continuous nanofiber bundles could be obtained. At a low rotation speed, the warping force of the horn is not able to drive the fibers into the yarns, and the higher the rotational speed, the higher the twist of the nanofiber yarns. In our experiments, samples with 100 rpm and 120 rpm were also, respectively. It was found that under 100 rpm, parallel fibrous bundles can be observed, and yarns have loose structures under 120 rpm, as shown in Fig. S1.† From about 150 rpm, the yarn twist is more applicable and hence we started the yarn preparation from 150 rpm. Also, the diameter of the fibrous yarns decreases as the horn rotation speed increases, as shown in Fig. 2a–d and S2,† which is because with the increasing rotating speed of the horn, the reel-stress for forming yarns during electrospinning increased; thus, more tightly twined yarns are generated. It is reported that sonication is useful in the deposition of nano-materials onto polymeric substrate.⁴⁴ In this work, sonication was done to deposit GR onto the fibrous yarns. During ultrasonic treatment, cavitation bubbles were formed around the ultrasonic amplitude transformer bar in DI water. When the cavitation bubbles approached the GR surface, microjets and shock waves were generated due to the collapse of some bubbles. GR was pushed toward the TPU fiber's surface with high speed by jets and shock waves with high energy. These high-energy forces caused the interfacial collision between GR and the TPU fibers.⁴⁵ Therefore, the TPU fibers softened or partially melted at the impacted sites during ultrasonication and resulted in GR anchoring onto the yarn's surface.

After ultrasonic treatment, the morphology of the GR/TPU yarns was slightly different from that of the original TPU yarns (Fig. 2e–h). This is due to the fact that the presence of GR nanosheets does not make the surface of the TPU fibers smooth enough. The surface of TPU fibers becomes rough like fish scales, which indicated that GR has been successfully fixed on the surface of TPU fibers (Fig. 2i–l). As shown in Fig. S3,† after ultrasonic treatment in GR solution, the white TPU yarns turned

black, indicating that graphene was anchored to the TPU fibers. Interestingly, GR could not only deposit on the outer layered fibers of the yarns but also permeate to the inner layer due to the presence of pores between the TPU fibers (Fig. S4†); thus, interconnected three-dimensional (3D) conductive networks can be constructed among the TPU yarns. Stress-strain tests were also performed on the GR/TPU yarns based on different rotational speeds. It can be seen that after the deposition of GR, the composites retained the outstanding mechanical property. As shown in Fig. S5,† it can be seen that the 150@GR/TPU yarn has the best tensile performance and can withstand up to 1400% tensile strain, and it decreases with increasing rotating speed. Interestingly, the 210@GR/TPU yarn, which has the lowest tensile properties, also meets the deformation requirements of wearable electronics by virtue of its mechanical properties.⁴⁶ The decreased tensile strength can be because with increasing rotating speed, higher reel-stress is applied on the fibrous yarns, and the stretching capability also damped accordingly. Also, the low loading of graphene significantly improved the mechanical properties of the composite because of the strong interfacial adhesion and the homogeneous dispersion between the graphene and TPU fibrous yarns.

Strain sensing performance

The current *versus* voltage (*I*–*V*) characteristics of GR/TPU yarns at different horn rotation speeds were measured. It was found that all *I*–*V* curves showed a linear relationship, and the slopes of these *I*–*V* curves decreased with increasing rotational speed (Fig. S6†). This is due to the fact that the diameter of the GR/TPU yarns becomes smaller with increasing rotational speed (Fig. 2), pores between individual fibers become small, and less graphene penetrates into the yarns, resulting in a gradual increase in the resistance of the GR/TPU yarns. Therefore, the following experiments have been conducted mainly based on the 150@GR/TPU yarns, which has the lowest resistance of $535 \Omega \text{ cm}^{-1}$



Fig. 2 (a) SEM images of 150@TPU yarns, (b) 170@TPU yarns, (c) 190@TPU yarns, and (d) 210@TPU yarns. SEM images of (e) 150@GR/TPU yarns, (f) 170@GR/TPU yarns, (g) 190@GR/TPU yarns, and (h) 210@GR/TPU yarns. High magnification SEM images of (i) 150@GR/TPU yarns, (j) 170@GR/TPU yarns, (k) 190@GR/TPU yarns, and (l) 210@GR/TPU yarns.

(Fig. S7†). In addition, the electrical conductance is also dependent on the ultrasound time. As shown in Fig. 3a, for the 150@GR/TPU yarns, with increasing ultrasonication time, the resistance drops drastically first and then becomes steady, and a platform is formed. The reason may be because at the beginning, GR tends to deposit onto the fibrous yarns with the increase in time; thus, the number of attached GR are more than the detached counterparts. On further increasing the ultrasound time, a dynamic equilibrium of the attached and detached GR could be formed, leading to a relatively stable electrical resistance. Besides, it was found that the I - V curves of 150@GR/TPU yarns exhibited a linear relationship from 0% to 140% strain, while other yarns can only reach a maximum of 100% (Fig. 3b and S8†). The decreased slope of these I - V curves with the increase in applied external strain indicates the change in the electrical resistance along with the deformation as well as the potential for strain sensing. To further evaluate the electromechanical performance of strain sensors, dynamic cyclic strain has

been proposed. Under a fixed strain of 100%, the resistance of the strain sensor changes at different tensile rates as follows.

$$\frac{\Delta R}{R_0} = \frac{(R - R_0)}{R_0}$$

where R_0 is the initial resistance and R is the real time resistance during the stretching process. As shown in Fig. 3c, the value of $\Delta R/R_0$ increases during tension and recovers when the tensile stress is withdrawn. The symmetrical output signals indicate that the resistance recovers at the same rate as the loading cycle, suggesting that the strain sensor is structurally stable. In addition, the maximum resistance change remains stable at different frequencies, indicating that the strain sensor is independent of the test frequency. Moreover, $\Delta R/R_0$ under different dynamic strain cycles has been studied under strains ranging from 1% to 20% and from 20% to 100%. From Fig. S9† and 3d, it can be seen that the maximum $\Delta R/R_0$ was always proportional to the applied strain.



Fig. 3 (a) Resistance value of 150@GR/TPU yarns at different ultrasonication times. (b) *I*–*V* curves of 150@GR/TPU yarns under 0–140% static strains. (c) *I*–*V* curves of 150@GR/TPU yarns under 0–100% dynamic strain at different rates. (d) *I*–*V* curves of 150@GR/TPU yarns under different dynamic strains. (e) Sensitivity variation of 150@GR/TPU yarns at 0–140% strain. (f) Schematic diagram of the structural changes in the GR/TPU yarns in the stretched condition. (g) 10 000 cycles of 150@GR/TPU yarns under 0–100% dynamic strain.

In addition to linearity, sensitivity is another important factor in characterizing the performance of strain sensors, which is inversely proportional to the applied strain (ϵ) as follows.⁴⁷

$$GF = \frac{\Delta R}{R_0 \epsilon}$$

Although there are reports on stretchable strain sensors with higher GF, most of them are restricted to a limited stretchability (usually $\epsilon < 30\%$).^{48,49} Also, high GF and high stretchability ($\epsilon > 50\%$) are required for human motion detection.⁵⁰ As shown in Fig. 3e, a GF of 7.08 is achieved when the strain is less than 100%, while it reaches 46.19 when the applied strain is greater than 100% because of the change in the structure of the conductive network for electron transport between GR. As shown in Fig. 3f, after ultrasonic treatment, a certain amount of GR is deposited on the surface of the twisted TPU fibers, which intertwine with each other to form a conductive network. When some strain is introduced, some GRs on a single TPU fiber are detached as the fibers shift into alignment, causing the resistance to rise, while other GR adhering to the surface of the TPU fibers are correspondingly shifted into alignment, resulting in direct, fast charge transfer. These two opposite mechanisms result in a slow increase in resistance and the resultant small GF (~ 7.08). When external strain is greater than 100%, the tight connection

between adjacent GR adhering to the surface of the TPU fibers will be separated, and the electrical conductive pathways decrease accordingly, resulting in a sharp increase in the resistance, obtaining a high GF = 46.19. Finally, when the applied strain is withdrawn, the sensor returns to its original state, the GRs are reconnected, and the resistance returns to its initial value. Our strain sensor possesses an optimal integration of a large strain range and a high GF, which facilitates the broadening of its applications, especially in large-scale human motion detection. Moreover, the strain sensor provides an excellent reliability and stability of its long-term performance as after over 10 000 dynamic stretch–release cycles between 0% and 100% strain (stretching speed: 1 cycle per s), the maximum values of the signals remained almost unchanged, demonstrating the superiority of our stretchable strain sensors (Fig. 3g). Table S1† summarizes the comparison between this work and other recently reported fabric-based sensors,^{18,35,40,51,52} from which it can be seen that our GR/TPU sensor has an impressively wide strain range and durability as well as a relatively low cost.

Human motion monitoring

The GR/TPU strain sensor has great potential for wearable electronics.⁵³ To demonstrate the potential application of GR/TPU-based strain sensors in this field, firstly, the GR/TPU yarn strain sensor was adopted to detect subtle movements of the

human body. As shown in Fig. S10,[†] we fixed the GR/TPU strain sensor to the skin near the eye and the mouth and the relative resistance changes of the eye blink and different facial expressions were tested, respectively. When the eyes are opened and closed, a rapid change in the relative resistance can be observed (Fig. S10a[†]) as well as that when the mouth was closed and opened (Fig. S10b[†]). Also, the changes in relative resistance with crying and laughing time were measured, as shown in Fig. S10c and d,[†] respectively. The above results demonstrated that the GR/TPU strain sensor has excellent performance in detecting subtle human movement. Furthermore, the fibrous yarns can also be woven into textiles. A strain-sensitive textile (strain sensor arrays) based on 150@GR/TPU yarns was fabricated, as shown in Fig. S11.[†] Under a voltage of 20 V, the strain sensor arrays generate different values of $\Delta R/R_0$ along with different bending angles (Fig. S12[†]); thus, the strain sensor arrays have potential applications in smart sensing. Next, the as-woven textile was used to monitor different human movements on various joints of the human body (Fig. 4a–c). With their flexibility and wide strain range, the sensor arrays have the capability to recognize a wide range of body movements, such as those of the wrist, elbow and knee joints, through electrical signal outputs. From Fig. 4d, when the wrist started to bend, the relative resistance became larger, and when the wrist returned

to its original shape, the relative resistance signal of the strain sensor almost quickly recovered to the initial value, illustrating the excellent performance. As shown in Fig. 4e and f, the fast response and regular relative resistance changes of the GR/TPU strain sensor provide it capability for monitoring a wide area of elbow and knee motion well. In addition, the relative resistance signals generated by different angles of such joints are also relatively different; thus, the motion of different joints can be easily recognized. Furthermore, the relative resistance changes of the bent wrist at different rates was tested. As shown in Fig. 4g, the wrist bending at different speeds produced different cycles of relative resistance changes, demonstrating that the GR/TPU strain sensors can detect motion at different speeds. A similar phenomenon was also observed when the elbow (Fig. 4h) and knee (Fig. 4i) moved at different speeds. The results demonstrate the capability of GR/TPU strain sensors in monitoring the motion of the human body, which has great potential for future smart clothing applications.

Position detection of an object on the textile

To evaluate the further application of GR/TPU composite yarns, textiles (sensor arrays) with high sensing accuracy have been introduced to detect the local pressure within the textile. As

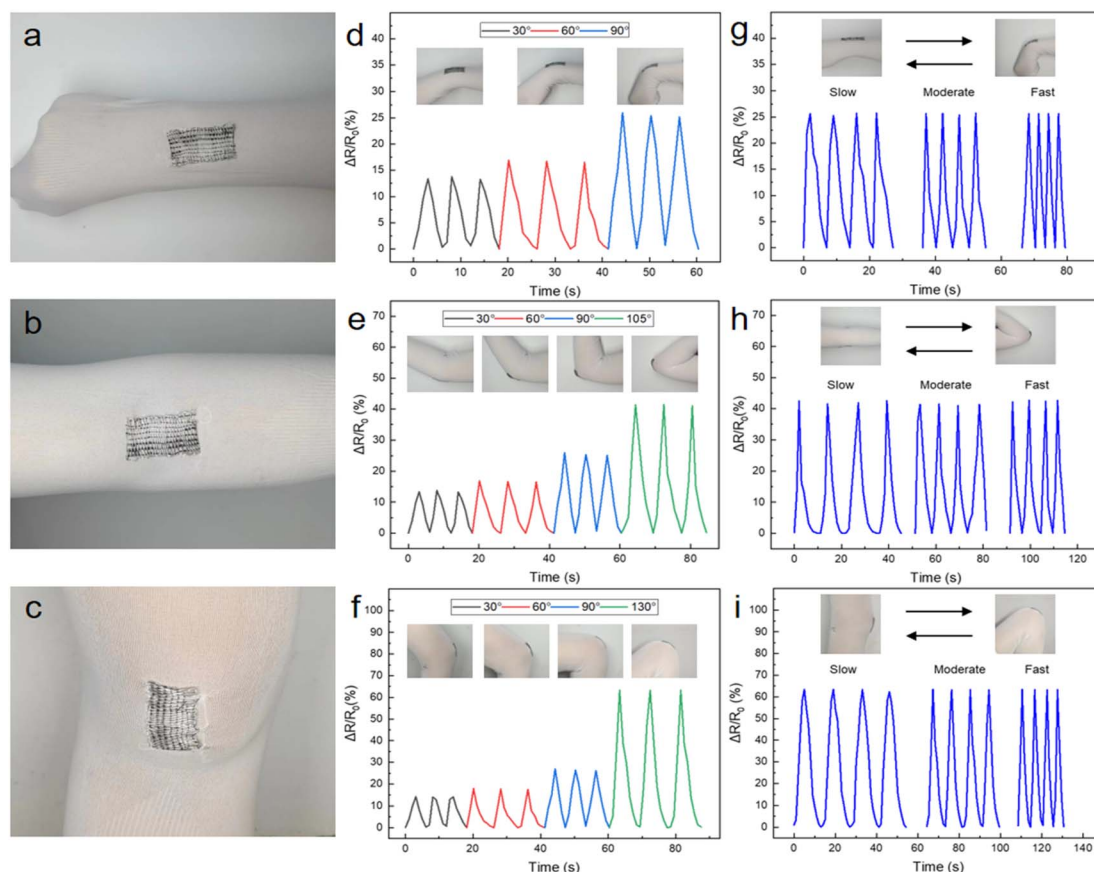


Fig. 4 Photographs of GR/TPU strain sensors fixed on the (a) wrist, (b) elbow and (c) knee. Variation of relative resistance at different bending angles of GR/TPU strain sensors fixed on the (d) wrist, (e) elbow and (f) knee. Changes in the relative resistance of GR/TPU strain sensors fixed on the (g) wrist, (h) elbow and (i) knee at different bending angles.



Fig. 5 (a) Photograph of the GR/TPU strain sensor array. (b–d) Signal from an array of strain sensors used to sense the position of the steel ball. (e) Temperature variation of the GR/TPU strain sensors at different voltages. (f) Infrared thermal image of a GR/TPU strain sensor at an operating voltage of 20 V.

shown in Fig. 5a, in this course, the GR/TPU yarns in the sensor array were termed as Y1 to Y3 according to the area. When a steel ball ($d = 1.67$ cm, $m = 28$ g) was placed at various locations of the textile, it was found that the resistance of the sensor arrays changed immediately; due to the change in the strain in both the longitudinal and transverse directions, it was observed that different relative resistance signals were generated by Y1, Y2, and Y3 when the balls were at different positions (Fig. 5b–d). It can clearly confirm the position where the small steel ball landed from it. Also, when the ball is taken away, the resistance can rapidly recover to its original value. Therefore, the position of the steel balls can be determined by accurately measuring the varying degrees of resistance changes in each portion of the textile. Finally, in order to ensure the safety of the sensor arrays for wearable devices, the temperature change within the operating voltage was measured. As shown in Fig. 5e and f, with increasing voltage, the surface temperature increases accordingly; however, the maximum temperature of the GR/TPU strain sensor is only 37.8 °C at the operating voltage (20 V). The temperature is within the safe range for human skin,⁵⁴ demonstrating the candidacy for safe wearables.

Conclusions

In summary, highly stretchable GR/TPU strain sensor based on one-step electrospun fibrous yarns was fabricated. The uniformly dispersed GR on TPU fiber surface can be connected with each other and formed integrated 3D electrical conductive networks. Due to the synergistic effect of variation of the distance between GRs and the geometrical changes during the deformation of the TPU yarns and the individual GR-wrapped fiber, the strain sensor demonstrates high sensitivity (GF of

7.08 in a strain of 100% and 46.19 in a strain of 140% in the reversible strain regime), good durability, and stability after more than 10 000 cycles of the stretching–releasing test. Textiles knitted by the strain sensors can be used for the real-time monitoring of human motion. Additionally, it can be adopted to accurately sense the precise position of an object on the textile. It is believed that the strain sensor can contribute to the next generation of wearable electronics.

Conflicts of interest

The authors declare no conflict of interest.

Acknowledgements

This study was supported by the Natural Science Foundation of Shandong Province (ZR2020ME193), and we thank Qingdao Nokang Environmental Protection Technology Co., Ltd for generously offering the electrospinning machine.

Notes and references

- 1 X. Liu, J. Miao, Q. Fan, W. Zhang, X. Zuo, M. Tian, S. Zhu, X. Zhang and L. Qu, *Adv. Fiber Mater.*, 2022, **4**, 361–389.
- 2 C. Wang, K. Xia, H. Wang, X. Liang, Z. Yin and Y. Zhang, *Adv. Mater.*, 2019, **31**, 1801072.
- 3 J. Lee, B. Llerena Zambrano, J. Woo, K. Yoon and T. Lee, *Adv. Mater.*, 2020, **32**, 1902532.
- 4 J. Xiong, J. Chen and P. S. Lee, *Adv. Mater.*, 2021, **33**, 2002640.
- 5 H. Liu, X. Chen, Y. Zheng, D. Zhang, Y. Zhao, C. Wang, C. Pan, C. Liu and C. Shen, *Adv. Funct. Mater.*, 2021, **31**, 2008006.

- 6 T. Raza, M. K. Tufail, A. Ali, A. Boakye, X. Qi, Y. Ma, A. Ali, L. Qu and M. Tian, *ACS Appl. Mater. Interfaces*, 2022, **14**, 54170–54181.
- 7 R. Yin, S. Yang, Q. Li, S. Zhang, H. Liu, J. Han, C. Liu and C. Shen, *Sci. Bull.*, 2020, **65**, 899–908.
- 8 Y. Tian, M. Huang, Y. Wang, Y. Zheng, R. Yin, H. Liu, C. Liu and C. Shen, *Chem. Eng. J.*, 2024, **480**, 147899.
- 9 T. Shen, S. Liu, X. Yue, Z. Wang, H. Liu, R. Yin, C. Liu and C. Shen, *Adv. Compos. Hybrid Mater.*, 2023, **6**, 127.
- 10 N. Tang, C. Zhou, D. Qu, Y. Fang, Y. Zheng, W. Hu, K. Jin, W. Wu, X. Duan and H. Haick, *Small*, 2020, **16**, 2001363.
- 11 Z. Chu, W. Jiao, Y. Huang, Y. Zheng, R. Wang and X. He, *J. Mater. Chem. A*, 2021, **9**, 9634–9643.
- 12 J. Eom, R. Jaisutti, H. Lee, W. Lee, J.-S. Heo, J.-Y. Lee, S. K. Park and Y.-H. Kim, *ACS Appl. Mater. Interfaces*, 2017, **9**, 10190–10197.
- 13 M. Liu, X. Pu, C. Jiang, T. Liu, X. Huang, L. Chen, C. Du, J. Sun, W. Hu and Z. L. Wang, *Adv. Mater.*, 2017, **29**, 1703700.
- 14 W. Yang, H. Liu, H. Du, M. Zhang, C. Wang, R. Yin, C. Pan, C. Liu and C. Shen, *Sci. China Mater.*, 2023, **66**, 2829–2842.
- 15 E. Samuel, B. Joshi, M.-W. Kim, Y.-I. Kim, M. T. Swihart and S. S. Yoon, *Chem. Eng. J.*, 2019, **371**, 657–665.
- 16 M. Tebyetekerwa, Z. Xu, W. Li, X. Wang, I. Marriam, S. Peng, S. Ramkrishna, S. Yang and M. Zhu, *ACS Appl. Energy Mater.*, 2018, **1**, 377–386.
- 17 S. Wu, T. Dong, Y. Li, M. Sun, Y. Qi, J. Liu, M. A. Kuss, S. Chen and B. Duan, *Appl. Mater. Today*, 2022, **27**, 101473.
- 18 T. Yan, Y. Wu, J. Tang and Z. Pan, *Mater. Res. Bull.*, 2021, **143**, 111452.
- 19 R. Ghosh, K. Y. Pin, V. S. Reddy, W. A. D. M. Jayathilaka, D. Ji, W. Serrano-García, S. K. Bhargava, S. Ramakrishna and A. Chinnappan, *Appl. Phys. Rev.*, 2020, **7**, 041309.
- 20 S. Hou, C. Chen, L. Bai, J. Yu, Y. Cheng and W. Huang, *Small*, 2023, 2306749.
- 21 X. Yue, Y. Jia, X. Wang, K. Zhou, W. Zhai, G. Zheng, K. Dai, L. Mi, C. Liu and C. Shen, *Compos. Sci. Technol.*, 2020, **189**, 108038.
- 22 C. Deng, L. Lan, P. He, C. Ding, B. Chen, W. Zheng, X. Zhao, W. Chen, X. Zhong, M. Li, H. Tao, J. Peng and Y. Cao, *J. Mater. Chem. C*, 2020, **8**, 5541–5546.
- 23 D. Zhang, M. Zhang, J. Wang, H. Sun, H. Liu, L. Mi, C. Liu and C. Shen, *Adv. Compos. Hybrid Mater.*, 2022, **5**, 1812–1820.
- 24 W. Hu, S. Chen, B. Zhuo, Q. Li, R. Wang and X. Guo, *IEEE Electron Device Lett.*, 2016, **37**, 667–670.
- 25 J. Li, S. Zhao, X. Zeng, W. Huang, Z. Gong, G. Zhang, R. Sun and C.-P. Wong, *ACS Appl. Mater. Interfaces*, 2016, **8**, 18954–18961.
- 26 M. Zhang, C. Wang, H. Wang, M. Jian, X. Hao and Y. Zhang, *Adv. Funct. Mater.*, 2017, **27**, 1604795.
- 27 G.-H. Lim, N.-E. Lee and B. Lim, *J. Mater. Chem. C*, 2016, **4**, 5642–5647.
- 28 H. Liu, J. Gao, W. Huang, K. Dai, G. Zheng, C. Liu, C. Shen, X. Yan, J. Guo and Z. Guo, *Nanoscale*, 2016, **8**, 12977–12989.
- 29 H. Liu, Y. Li, K. Dai, G. Zheng, C. Liu, C. Shen, X. Yan, J. Guo and Z. Guo, *J. Mater. Chem. C*, 2016, **4**, 157–166.
- 30 S. Li, J. G. Park, S. Wang, R. Liang, C. Zhang and B. Wang, *Carbon*, 2014, **73**, 303–309.
- 31 L. S. Cai, P. Luan, Q. Zhang, N. Zhang, Q. Gao, D. Zhao, X. Zhang, M. Tu, F. Yang, W. Zhou, Q. Fan, J. Luo, W. Zhou, P. M. Ajayan and S. Xie, *Sci. Rep.*, 2013, **3**, 3048.
- 32 J. Zhao, G. Wang, R. Yang, X. Lu, M. Cheng, C. He, G. Xie, J. Meng, D. Shi and G. Zhang, *ACS Nano*, 2015, **9**, 1622–1629.
- 33 Y. Cheng, R. Wang, J. Sun and L. Gao, *Adv. Mater.*, 2015, **27**, 7365–7371.
- 34 L. Yu, J. C. Yeo, R. H. Soon, T. Yeo, H. H. Lee and C. T. Lim, *ACS Appl. Mater. Interfaces*, 2018, **10**, 12773–12780.
- 35 W. Zhong, C. Liu, C. Xiang, Y. Jin, M. Li, K. Liu, Q. Liu, Y. Wang, G. Sun and D. Wang, *ACS Appl. Mater. Interfaces*, 2017, **9**, 42058–42066.
- 36 M. Amjadi, A. Pichitpajongkit, S. Lee, S. Ryu and I. Park, *ACS Nano*, 2014, **8**, 5154–5163.
- 37 S. Yao and Y. Zhu, *Nanoscale*, 2014, **6**, 2345–2352.
- 38 H. Liu, Q. Li, S. Zhang, R. Yin, X. Liu, Y. He, K. Dai, C. Shan, J. Guo, C. Liu, C. Shen, X. Wang, N. Wang, Z. Wang, R. Wei and Z. Guo, *J. Mater. Chem. C*, 2018, **6**, 12121–12141.
- 39 X. Huang, C. Zhi, Y. Lin, H. Bao, G. Wu, P. Jiang and Y.-W. Mai, *Mater. Sci. Eng., R*, 2020, **142**, 100577.
- 40 S. Wang, H. Ning, N. Hu, Y. Liu, F. Liu, R. Zou, K. Huang, X. Wu, S. Weng and Alamusi, *Adv. Mater. Interfaces*, 2020, **7**, 1901507.
- 41 J. He, K. Qi, Y. Zhou and S. Cui, *J. Appl. Polym. Sci.*, 2014, **131**, app.40137.
- 42 U. Ali, H. Niu, A. Abbas, H. Shao and T. Lin, *RSC Adv.*, 2016, **6**, 30564–30569.
- 43 U. Ali, Y. Zhou, X. Wang and T. Lin, *J. Text. Inst.*, 2012, **103**, 80–88.
- 44 H. Shi, D. Shi, L. Yin, Z. Yang, S. Luan, J. Gao, J. Zha, J. Yin and R. K. Y. Li, *Nanoscale*, 2014, **6**, 13748–13753.
- 45 J. Gao, M. Hu, Y. Dong and R. K. Y. Li, *ACS Appl. Mater. Interfaces*, 2013, **5**, 7758–7764.
- 46 R. Ghosh, K. Y. Pin, V. S. Reddy, W. A. D. M. Jayathilaka, D. Ji, W. Serrano-García, S. K. Bhargava, S. Ramakrishna and A. Chinnappan, *Appl. Phys. Rev.*, 2020, **7**, 041309.
- 47 J. F. Christ, N. Aliheidari, A. Ameli and P. Pötschke, *Mater. Des.*, 2017, **131**, 394–401.
- 48 Y. Tang, Z. Zhao, H. Hu, Y. Liu, X. Wang, S. Zhou and J. Qiu, *ACS Appl. Mater. Interfaces*, 2015, **7**, 27432–27439.
- 49 D. Y. Wang, L. Q. Tao, Y. Liu, T. Y. Zhang, Y. Pang, Q. Wang, S. Jiang, Y. Yang and T. L. Ren, *Nanoscale*, 2016, **8**, 20090–20095.
- 50 S. Gong, D. T. H. Lai, B. Su, K. J. Si, Z. Ma, L. W. Yap, P. Guo and W. Cheng, *Adv. Electron. Mater.*, 2015, **1**, 1400063.
- 51 T. Huang, P. He, R. Wang, S. Yang, J. Sun, X. Xie and G. Ding, *Adv. Funct. Mater.*, 2019, **29**, 1903732.
- 52 X. Wang, Y. Qiu, W. Cao and P. Hu, *Chem. Mater.*, 2015, **27**, 6969–6975.
- 53 Z. Wang, Y. Huang, J. Sun, Y. Huang, H. Hu, R. Jiang, W. Gai, G. Li and C. Zhi, *ACS Appl. Mater. Interfaces*, 2016, **8**, 24837–24843.
- 54 C. Tan, Z. Dong, Y. Li, H. Zhao, X. Huang, Z. Zhou, J.-W. Jiang, Y.-Z. Long, P. Jiang, T.-Y. Zhang and B. Sun, *Nat. Commun.*, 2020, **11**, 3530.